ELSEVIER

Biochimica et Biophysica Acta 1233 (1995) 89–104

BBA Biochimica et Biophysica Acta

Calorimetric and theoretical studies of the effects of lindane on lipid bilayers of different acyl chain length

Mads C. Sabra, Kent Jørgensen, Ole G. Mouritsen *,[1]

Department of Physical Chemistry, Technical University of Denmark, Bldg. 206, DK-2800 Lyngby, Denmark

Received 17 June 1994; accepted 6 October 1994

Abstract

The effects of the insecticide lindane on the phase transition in multilamellar bilayers of saturated diacylphosphatidylcholines of different acyl chain length ($DC_{14}PC$, $DC_{16}PC$, and $DC_{18}PC$) have been studied by means of differential scanning calorimetry (DSC), as well as computer-simulation calculations on a molecular interaction model. The calorimetric data show that increasing concentrations of lindane lower the transition temperature and lead to a broadening of the specific heat in a systematic way depending on the lipid acyl chain length. Kinetic effects in the observed calorimetric traces indicate that the incorporation of lindane into multilamellar lipid bilayers is slow, but faster for the shorter lipid species. Large unilamellar vesicles do not show such kinetic effects. The transition enthalpy is for all three lipid species found to be independent of the lindane concentration which implies that the entropy of mixing is vanishingly small. This lends support to a microscopic molecular interaction model which assigns the absorbed lindane molecules to interstitial sites in the bilayer. Computer-simulation calculations on this model, which assumes a specific interaction between lindane and certain excited acyl chain configurations, lead to predictions of the lipid–water partition coefficient in qualitative agreement with experimental measurements (Antunes-Madeira and Madeira (1985) Biochim. Biophys. Acta 820, 165–172). The partition coefficient has a peak near the phase transition which is a consequence of enhanced interfacial adsorption of lindane at lipid-domain interfaces.

Keywords: Lindane; Phospholipid bilayer; Partition coefficient; Kinetic effect; Calorimetry; Computer simulation

1. Introduction

Considerable effort has been devoted to elucidate the molecular mechanisms responsible for the toxic effects of insecticides [1,2] such as DDT, lindane, parathion, and malathion. These compounds are generally non-polar and it is therefore expected that their site of action is at the lipid-bilayer component of the cell membrane, in particular at the membranes of nerve cells. It is still an unsettled question whether specific membrane receptors are involved in the toxic action or if the lipid bilayer is a target for the insecticides. In this sense, the situation resembles that of general anaesthesia and the effects of various drugs and alcohols on biological membranes [3] where a similar controversy exists regarding the molecular mechanisms involved. In order to clarify the problem of insecticide action it is important to carry out systematic studies on well-defined model systems involving synthetic lipid bilayers and native membranes by which it is possible to quantitatively characterize the effects of the insecticide on the bare physicochemical properties of the membrane. Such information will be essential for making further progress in our understanding of the molecular mechanisms of the toxic action of insecticides in living cells.

A substantial body of experimental literature exists on the change in the physicochemical properties of simple membrane systems due to the interaction with insecticides, such as lindane [1,4–6], DDT [1,7–11], parathion [12,13], and malathion [14]. In particular the group of Antunes-Madeira and Madeira [4–6,10–14] has made a series of systematic studies using different techniques involving ra-

Abbreviations: DC_nPC, saturated diacylphosphatidylcholine with n carbon atoms in each acyl chain; DSC, differential scanning calorimetry; lindane, γ-1,2,3,4,5,6-hexachlorocyclohexane.

* Corresponding author. E-mail: fymearn@vm.uni_c.dk. Fax: +45 45 934808.

[1] O.G.M. is an Associate Fellow of the Canadian Institute for Advanced Research.

SSDI 0005-2736(94)00244-4

dioactive labelling and fluorescence spectroscopy leading to information on partition coefficients and the influence of insecticides on membrane structure and fluidity.

In the present paper we are going to study the effects of lindane on synthetic phospholipid bilayers using a combined experimental and theoretical approach, involving DSC and computer-simulation calculations on a molecular interaction model. The influence of lindane on lipid-bilayer properties has not been studied previously with any of these techniques. The combined approach leads to a detailed picture of the way lindane interacts with the lipid bilayer. Similar to a large number of previous studies of the interaction of membrane-active molecular agents with lipid bilayers, we shall focus on the gel–fluid main phase transition of phospholipid bilayers [15] and investigate how the interaction of the active molecules with the bilayer manifests itself in alterations of the transitional properties.

Different effects of the interactions between lipid bilayers and lindane have been studied by radioactive labelling [4] and fluorescence spectroscopy [1] to determine the partitioning of lindane between the lipid bilayer and the aqueous phase. Fluorescence spectroscopy has also been used to evaluate the bilayer fluidity changes that are induced by lindane [5,6]. It has been reported that the partitioning in the gel phase is very low and considerably higher in the fluid phase [4]. Furthermore, the incorporation of lindane into the lipid bilayer was found to increase and display a broad maximum in a temperature range around the main transition. This enhanced absorption in the transition region was found to increase with decreasing acyl chain length of phospholipids in the series $DC_{14}PC$, $DC_{16}PC$, and $DC_{18}PC$. The fluorescence spectroscopic studies showed that lindane tends to broaden the phase transition and shift it to lower temperatures [5]. The lipid acyl chain order in the gel phase was found to decrease whereas lindane showed no discernable effect in the fluid phase. Cholesterol in large amounts was found to reverse the disordering effect of lindane in the gel phase [5]. Similar effects have been observed for other insecticides, such as DDT [11], malathion [14], and parathion [13].

Guided by these and related results for the effect of certain local and general anaesthetics on phospholipid bilayers [16], a general molecular interaction model has been proposed to account for the effect of insecticides on the physical properties of lipid bilayers [17,18]. The results from computer-simulation calculations on the model suggested that the increased absorption of insecticides in lipid bilayers may be explained by the occurrence and enhancement of dynamic bilayer heterogeneity in the transition region [19,20]. Dynamic heterogeneity implies formation of lipid domains and interfaces between the lipid domains and the bulk bilayer phase. The domain interfaces act as sinks for the insecticides. We shall in this paper elaborate further on this picture and demonstrate how it is capable of accounting for the systematics of lindane effects on phospholipid bilayers with different chain length, specifically $DC_{14}PC$, $DC_{16}PC$, and $DC_{18}PC$.

2. Materials and experimental methods

2.1. Preparation of multilamellar vesicles

Multilamellar vesicles of each of the phospholipids $DC_{14}PC$, $DC_{16}PC$, and $DC_{18}PC$ were prepared, one at the time, by suspending 25 μmol pure dry lipid into 5.00 ml of a KCl solution consisting of 50 mM KCl and 1.0 mM NaN_3. The resulting suspension was heated to about 20°C above the transition temperature, T_m, for the lipid species in question. The temperature of the suspension was kept constant for at least 1 h. Every 15 min the suspension was shaken vigorously by vortexing. The final lipid concentration was 5 mM. The dispersions were then stored at 5°C.

2.2. Preparation of unilamellar vesicles

Large unilamellar vesicles of $DC_{16}PC$ were prepared from the multilamellar vesicles by standard extrusion techniques [21]. Ten repeated extrusions through two stacked membranes of pore size 100 nm were performed.

2.3. Preparation of lindane solution

A saturated lindane solution was prepared by adding 50 μmol dry lindane to 1000 ml of the KCl solution mentioned above, and then heating to 60–80°C for several hours, before cooling to room temperature (22°C). Only a minor part of the added lindane was not dissolved by this procedure. We have not determined the absolute lindane concentration in the saturated solution. Previous work has indicated that the lindane concentration at saturation is 25 μM [22] but larger values have also been quoted [23]. Hence, we conclude that the absolute concentration in our saturated lindane solution is in the range 25–50 μM. For convenience, we shall here denote the lindane concentration in the lipid samples to be described below in terms of a percentage of saturation (%sat.), i.e., the percentage of the sample volume that is made up of the saturated lindane solution. This is an internally consistent and well-defined measure which allows a systematic comparison between different types of lipids.

2.4. Preparation of samples

Samples for DSC studies were prepared at room temperature (22°C) immediately before scanning by mixing lipid dispersion with lindane solution and KCl solution to obtain a final lipid concentration of 200 μM and lindane concentrations of 0%, 24%, 48%, 72% and 96% of saturation. The samples were vortexed shortly before they were loaded into the calorimeter. This type of sample prepara-

tion where lindane is added from the aqueous phase rather than by co-solubilization was chosen in order to be able to control the lindane content in the aqueous phase.

2.5. Differential scanning calorimetry

Differential scanning calorimetry was performed using a MC-2 Ultrasensitive Scanning Calorimeter from Microcal (Northhampton, MA, USA). The calorimeter is of the power-compensating type with cell volumes of 1.2 ml. During scanning the reference cell contained the KCl solution. Three or more successive upscans were performed on each sample. The scanned temperature ranges were 17–27°C for $DC_{14}PC$, 35–45°C for $DC_{16}PC$, and 50–60°C for $DC_{18}PC$. The scan rate was always 13°C/h. Before the beginning of each scan, the sample was equilibrated during 50 min at the starting temperature. Immediately after the end of a scan the system was cooled to the starting temperature of the following scan in order to equilibrate. The samples were subject to a hydrostatic pressure of about 3 atm. (absolute) during scanning. In the DSC experiment the excess heat capacity is measured. We shall throughout this paper refer to this quantity as the specific heat, C_p.

2.6. Reagents

$DC_{14}PC$, $DC_{16}PC$, and $DC_{18}PC$, at least 99% pure, were obtained from Avanti Polar Lipids. Lindane was obtained from Sigma and was of commercial grade. All reagents were used without further purification.

2.7. Data analysis

MicroCal Origin™ software was used to subtract appropriate baselines from the obtained excess specific-heat curves and subsequently used to integrate the curves and to determine the peak position, T_m, and the peak width at half maximum, $T_{1/2}$.

3. Microscopic model and calculational techniques

3.1. Microscopic model

The microscopic model that we use to describe the partitioning of lindane into lipid bilayers and the interaction between lindane and the lipid molecules is the one proposed by Jørgensen et al. [17,18] for lipid–insecticide interactions. This model is an extension of the ten-state model by Pink et al. [24] used to describe the transitional properties of phospholipid bilayers [25]. Within this model the acyl chains of the phospholipids are situated on a triangular lattice. The lattice is a mere topological construction which assures that each lipid chain has six nearest neighbors which, however, need not be in the same distance from the chain in question. The lindane molecules are interstitially intercalated between the acyl chains. Hence the absorption sites for lindane formally form a honeycomb lattice imbedded in the triangular lipid lattice. Since, by this construction, the lindane molecules and the lipid molecules exist on separate lattices, the entropy of mixing is automatically zero, which is consistent with our experimental findings (cf. Section 4). Within this model no specification is made of the actual position of the lindane molecules in the lipid hydrophobic bilayer core. The Pink model distinguishes between different acyl chain states, $m = 1, 2, \ldots, 10$, each characterized by an internal conformational energy, E_m, a cross-sectional area, A_m, and a degeneracy, D_m, which is related to a single-chain entropy. The 10 states include the $m = 1$ fully ordered state (the all-*trans* state), the $m = 10$ disordered (fluid) state, together with eight intermediate states characterized by a certain degree of acyl chain disorder. The model includes only nearest-neighbour interactions: lipid–lipid, lipid–lindane, and lindane–lindane, characterized by the interaction constants J_{LL}, J_{LA}^m, and J_{AA}. We have explicitly assumed that the lindane molecule interacts in a selective way with the lipid acyl chain, i.e., in a way that depends on the conformational state, m, of the chain.

The energetics of the model is described by the effective Hamiltonian

$$\begin{aligned}\mathcal{H} = & \sum_i \sum_{m=1}^{10} (E_m + \Pi A_m)\mathcal{L}_{mi} \\ & - \frac{J_{LL}}{2} \sum_{\langle i,j \rangle} \sum_{m,n=1}^{10} I_m I_n \mathcal{L}_{im}\mathcal{L}_{jn} \\ & + \sum_i \sum_{m=1}^{10} \sum_l J_{LA}^m \mathcal{L}_{im}\mathcal{L}_l^A \\ & - \frac{J_{AA}}{2} \sum_{\langle l,k \rangle} \mathcal{L}_l^A \mathcal{L}_k^A - \mu \sum_l \mathcal{L}_l^A \end{aligned} \quad (1)$$

where $\mathcal{L}_{im} = 0, 1$ is a variable indicating the conformational state of the chain at site i of the lipid lattice and $\mathcal{L}_l^A = 0, 1$ is a variable indicating the occupancy of the lth site of the lindane lattice. I_m is a nematic shape factor [25]. $\Pi = 30$ dyne/cm (i.e., $3 \cdot 10^{-2}$ N/m) is an interfacial pressure added to assure bilayer stability [25]. The model parameters for pure phospholipid bilayers with different acyl chain length, which have previously been discussed by Ipsen et al. [26], are given in Table 1. The interaction constants, J_{LA}^m, initially chosen for the lipid–lindane inter-

Table 1
Parameters for the ten-state Pink model in Eq. (1)

Phospholipid	$E_{10}/10^{-13}$ erg	D_{10}	$J_{LL}/10^{-13}$ erg
$DC_{14}PC$	1.94	6×3^8	0.618
$DC_{16}PC$	2.78	6×3^{10}	0.709
$DC_{18}PC$	3.62	6×3^{12}	0.815

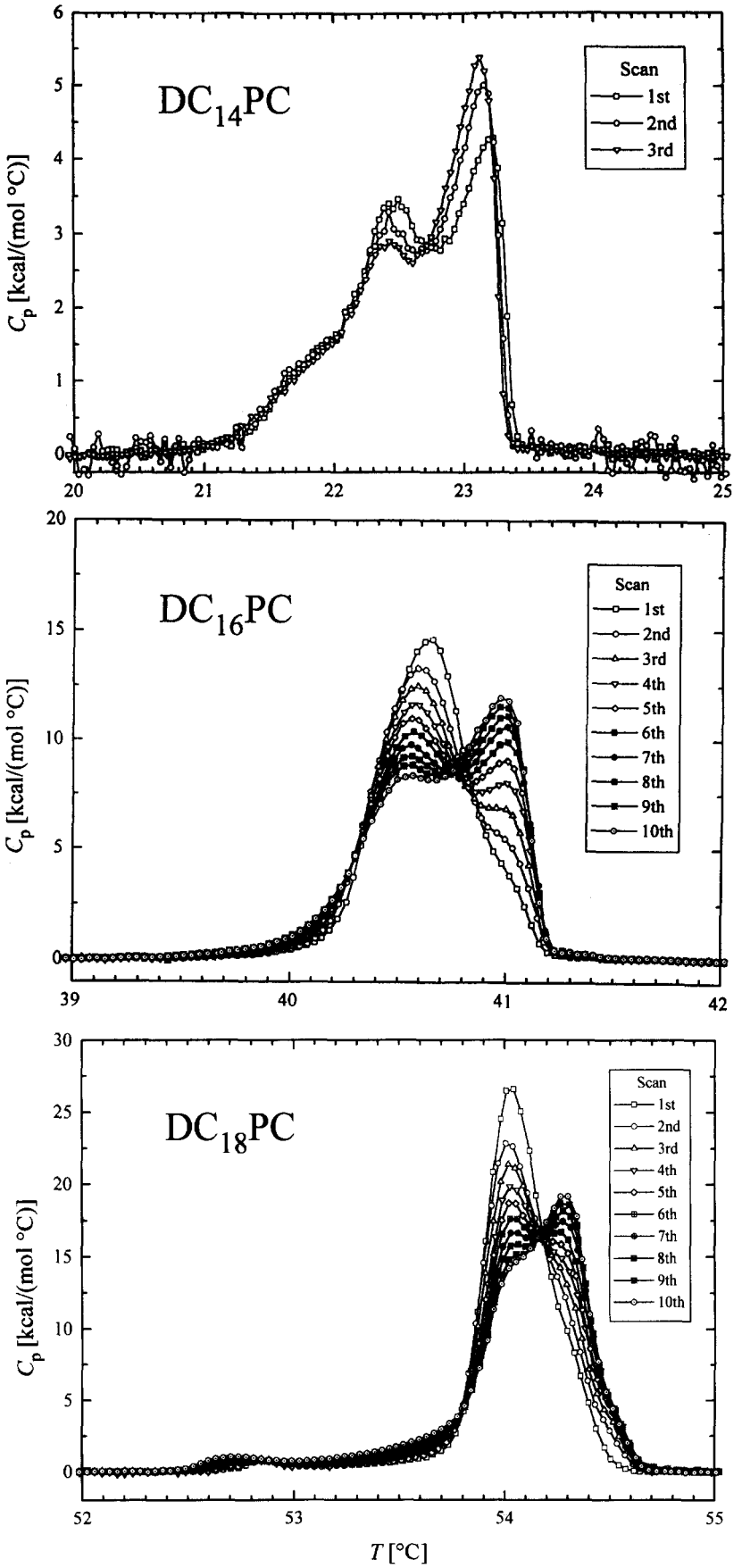
DC14PC
Scan
1st
2nd
3rd
Cp [kcal/(mol °C)]
DC16PC
Scan
1st
2nd
3rd
4th
5th
6th
7th
8th
9th
10th
Cp [kcal/(mol °C)]
DC18PC
Scan
1st
2nd
3rd
4th
5th
6th
7th
8th
9th
10th
Cp [kcal/(mol °C)]
T [°C]

actions are given in Table 2. The values reflect a weak repulsion to the all-trans state, a stronger repulsion to the lower-lying gel-like states, whereas there is an attractive interaction between lindane and some of the more excited chain states that involve kink formation. This selective interaction between lindane and certain lipid chain states reflect a steric interaction corresponding to the assumption that the lindane molecules fit better to certain chain conformations (e.g., those involving kinks) [18]. Lindane is assumed to have a weakly attractive interaction with the fluid state. Other values of these parameters will be considered in Section 5. Finally, the interaction constant for lindane–lindane interactions is chosen as slightly attractive, $J_{AA} = 0.1 \cdot 10^{-13}$ erg (i.e., 10^{-21} joule). It should be noted that all these interaction constants are effective, and use of terms like attractive and repulsive should be considered in a relative sense. It should be pointed out that the interaction parameters involving lindane is not known a priori (cf. Section 5).

The concentration, x, of lindane molecules in the bilayer is not a conserved quantity since a partitioning between the membrane and the aqueous phase is assumed to occur. The partitioning is controlled by the chemical potential, μ, in the last term in Eq. (1). Hence the modelling refers to the grand canonical ensemble. The natural concentration variable for lindane in the bilayer is

$$x = \frac{2\langle \mathscr{L}_l^A \rangle}{1 + 2\langle \mathscr{L}_l^A \rangle} \tag{2}$$

since there are two interstitial lindane sites per lipid acyl chain. The standard molar concentration, y, is related to x as

$$y = 2x/(1+x) \tag{3}$$

since each lipid molecule carries two acyl chains.

3.2. Calculational method

Standard Monte Carlo computer-simulation techniques [25] have been used to determine the thermodynamic equilibrium properties of the model described by the Hamiltonian in Eq. (1). The simulations are performed on lattices composed of 60×60 lipid acyl chain sites and 60×2 interstitial lindane sites. The lattices are subject to periodic boundary conditions. This system size is estimated to be sufficiently large to represent the thermodynamic limit for the quantities presented below. The simulations provide an equilibrium ensemble of configurations by using Glauber dynamics [25] for both acyl chain excitations and lindane partitioning. The equilibrium properties are obtained by averaging over ensembles consisting of about 10^8 system configurations. In the computer simulations the specific heat is conveniently calculated via the fluctuation–dissipation theorem

$$C_p = \left(k_B T^2\right)^{-1} \left(\langle \mathscr{H}^2 \rangle - \langle \mathscr{H} \rangle^2\right). \tag{4}$$

4. Experimental results

4.1. Kinetics of lindane incorporation

Successive upscans were performed on each lipid–lindane sample as described in Section 2.4. Selected results for a series of successive scans are shown in Fig. 1 for all three lipid species. The complete set of specific-heat data obtained in the last scan for each sample investigated, including the three pure lipid samples of $DC_{14}PC$, $DC_{16}PC$, and $DC_{18}PC$, is given in Fig. 2. We shall refer to the data in Fig. 2 as the 'equilibrium data' and return to a discussion thereof in Section 4.2. It is noted that for all three lipid species the presence of lindane in the sample leads to a freezing-point depression and a progressive broadening of the transition. However, Fig. 1 shows that the data is subject to very significant kinetic effects. For $DC_{14}PC$ the effects are marginal and basically within the experimental noise but they become significant in the case of $DC_{16}PC$ and $DC_{18}PC$. The kinetic effects are stronger the higher the lindane concentration is. It should be noted from Fig. 1 that the kinetic effects occur over a temperature range that is less than 1°C.

For the $DC_{16}PC$ and $DC_{18}PC$ systems ten successive scans were performed. Already the first of the ten excess specific-heat curves shows properties which differ from the curve for the pure system, cf. Fig. 1, which showed no significant dependence on the number of scans performed at the used scan rate. Apart from being broadened and shifted to lower temperatures, the specific-heat curve for the first scan displays a small shoulder at the high-temperature side. During the following scans, the intensity of this shoulder increases, simultaneously with a decrease in the intensity of the main peak. Eventually, the shoulder turns into a peak so that the specific-heat curve now contains two peaks. The original peak then decreases further in intensity as the new peak increases in intensity. In the case of the $DC_{18}PC$ systems the decrease in the intensity of the original peak is so strong, that the peak finally turns into a shoulder of the new peak. The same is observed for $DC_{16}PC$ samples with lower lindane contents, whereas the

Fig. 1. Evolution during successive upscans of the specific heat obtained by DSC for multilamellar bilayers samples of 200 μM $DC_{14}PC$, $DC_{16}PC$, and $DC_{18}PC$ containing lindane. The lindane concentration in the three systems corresponds to 72% sat., 72% sat., and 96% sat., respectively. Note the difference in scales for the different lipids.

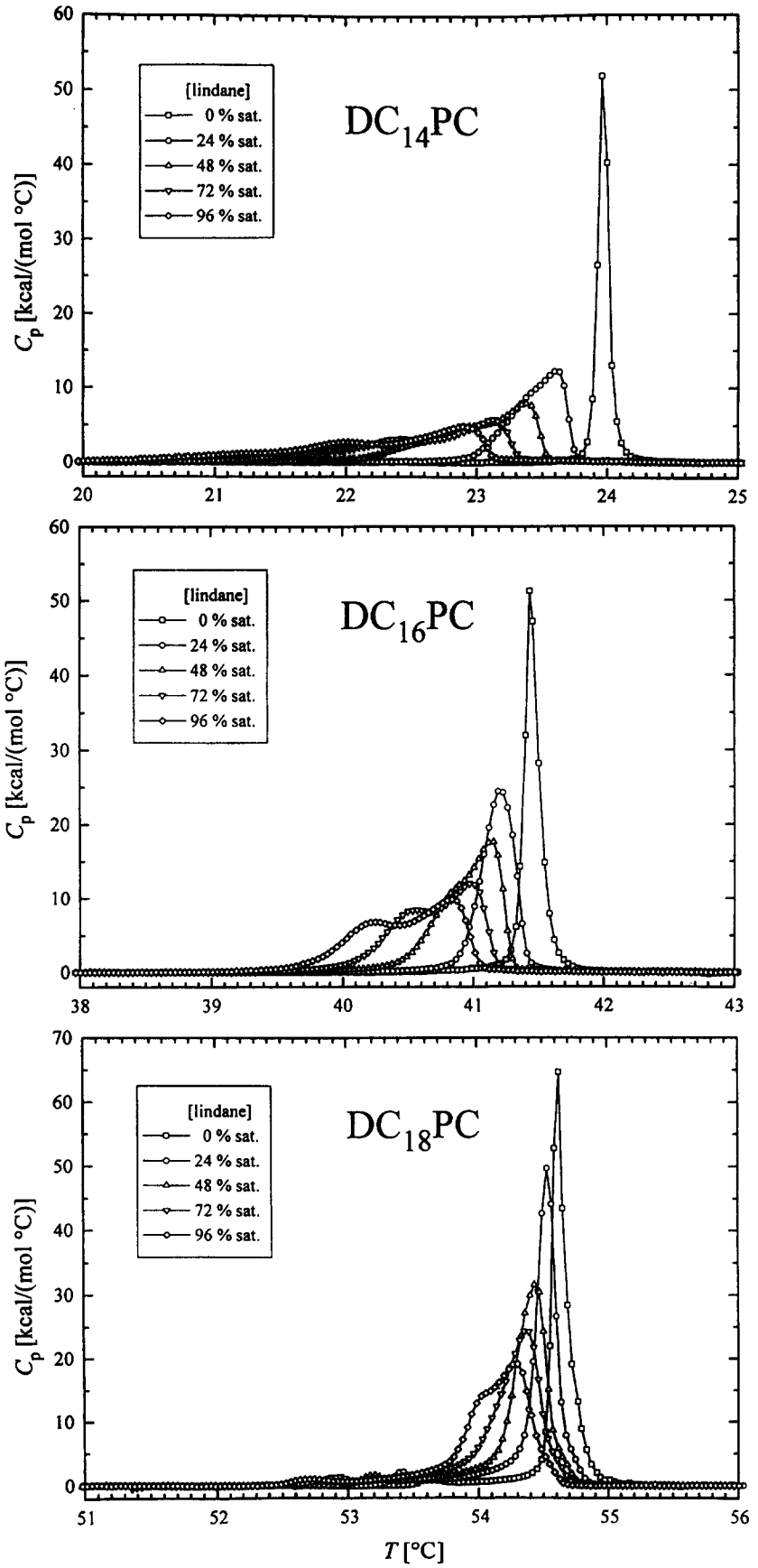

Fig. 2. Specific-heat curves from the last ('equilibrium data') of a series of upscans, cf. Fig. 1, obtained by DSC shown together with the specific heat of pure $DC_{14}PC$, $DC_{16}PC$, and $DC_{18}PC$ systems. Results for different lindane concentrations are shown.

Table 2
Parameters for the lipid–lindane interactions in Eq. (1)

m	J^m_{LA} /10^{-13} erg
1	−0.20
2	−2.00
3	−2.00
4	−2.00
5	0.24
6	0.24
7	0.24
8	0.24
9	0.24
10	0.06

final excess specific-heat curves of $DC_{16}PC$ samples with higher lindane contents have two distinct peaks. Another, but much weaker development is observed in the low temperature wing of the specific heat. During successive scans the intensity of the wing increases. This development is observed for all $DC_{16}PC$ and $DC_{18}PC$ samples containing lindane including those with only 24% sat. lindane, which do not show the described development of the shoulder in the high-temperature region of the peak.

The series of successive upscans for the $DC_{16}PC$ sample containing lindane in a concentration of 48% saturation was interrupted after the sixth scan. The sample was then allowed to rest at 20°C in the calorimeter for approximately 2 hours, before six more scans were performed. Some of these scans are presented in Fig. 3. The seventh scan, i.e., the first one after the resting period, showed a marked deviation from the development of the $DC_{16}PC$ data shown in Fig. 1. The intensity of the high-temperature peak is much higher than would be expected from Fig. 1 and similarly the position of this peak occurs at higher temperatures. The last five scans, which show only little development, conform however reasonably well with what one would have expected based on the data in Fig. 1. The same type of interruption in the series of upscans for a $DC_{18}PC$ sample with 72% sat. lindane showed a behavior qualitatively similar to that of $DC_{16}PC$ in Fig. 3, although less pronounced.

In order to provide a quantitative measure the kinetic development of the specific-heat curves in Fig. 2, we subtract the specific-heat curve of the first scan from each of those of the subsequent scans and determine the corresponding series of area differences that are due to the increased intensity of the high-temperature shoulder/peak. The calculated areas are divided by the average area of the full specific-heat function in order to obtain a measure of the relative development which we denote by δh. Results for δh derived from this procedure are presented in Fig. 4. The rate of development is seen to be largest in the first few scans and then to decrease slowly in the following scans. The rates are larger for $DC_{16}PC$ than for $DC_{18}PC$, and an increased concentration of lindane leads to a larger rate and to a slower decrease of the rate during the later scans.

Finally, the development of the area under the full specific-heat curves was investigated. The results are presented in Fig. 5. The total area, which corresponds to the transition enthalpy, ΔH, increases as the scans proceed. It seems in the case of $DC_{16}PC$ that the value of ΔH saturates and levels out after 6–8 scans and that 'equilibrium' has hence been attained. This is particularly clear

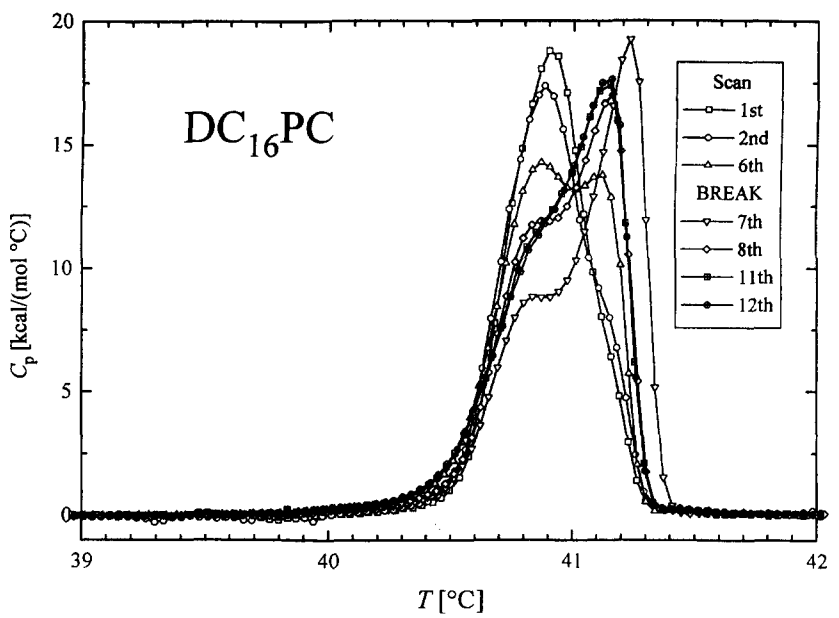

Fig. 3. Evolution during successive DSC upscans of the specific heat for multilamellar bilayers samples of 200 μM $DC_{16}PC$ containing lindane in a concentration corresponding to 48% sat. This series of upscans were interrupted after the 6th scan and the sample were put to rest in the calorimeter at 20°C for approx. 2 h before the next six scans were performed.

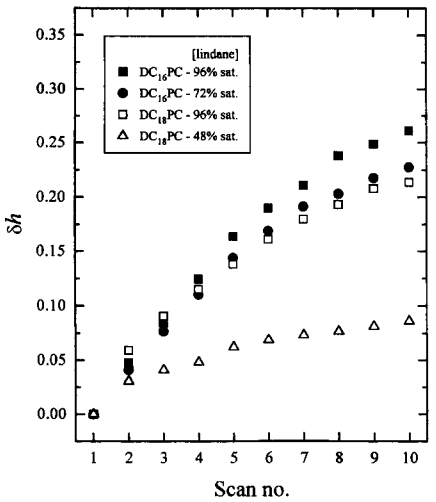

Fig. 4. Evolution of the relative heat increase, δh, of the high-temperature specific-heat peaks in Fig. 1 as a function of number of DSC upscans on various different multilamellar lipid-lindane systems. δh is defined as the increase in area under the high-temperature peak/shoulder relative to the first scan divided by the total heat content in the specific heat function.

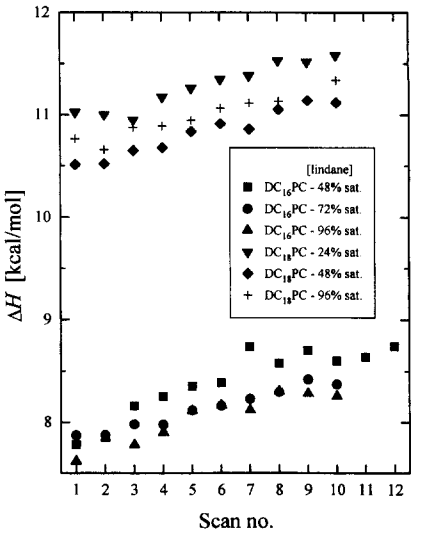

Fig. 5. Evolution of the total heat content, ΔH (the equilibrium transition enthalpy), as a function of the number of DSC upscans obtained from the specific-heat functions for multilamellar $DC_{16}PC$ and $DC_{18}PC$ bilayer systems with different contents of lindane.

in the case of the scan series for the $DC_{16}PC$ sample with 48%sat. lindane subject to the interruption procedure and a resting period where the data for ΔH in Fig. 5 seems to have leveled out.

We shall in Section 6 return to a discussion and interpretation of the results on the kinetic effects in the specific heat in terms of a model for the incorporation of lindane into multilamellar lipid bilayers.

4.2. Equilibrium studies

We shall now present the thermodynamic data that can be obtained from the specific-heat curves of the last of the successive scans performed on each of the different samples, cf. Fig. 2. For convenience we refer to these data as 'equilibrium data', although it is likely that the samples are not in truly thermodynamic equilibrium as will be discussed in Section 5.

In the case of the $DC_{14}PC$ sample containing 24% sat. lindane the specific heat function in Fig. 2 is much broader and peaks at a somewhat lower temperature than the specific-heat curve for the pure system. Part of the broadening is due to the presence of a shoulder in the low-temperature region of the peak. In the system containing 48% sat. lindane, the broadening and the shift of the transition are even more pronounced and the shoulder has turned into a separate peak. This behavior is enhanced when the lindane concentration is increased. Possibly a third low-temperature feature in terms of a shoulder on the low-temperature side of the specific heat has developed for the highest concentrations, see Fig. 1. Similar observations are made for the $DC_{16}PC$ and $DC_{18}PC$ samples, although to a somewhat lesser extent. In the case of $DC_{18}PC$ the low-temperature peak is absent even for the system containing 96% sat. lindane.

We define the transition temperature of a sample con-

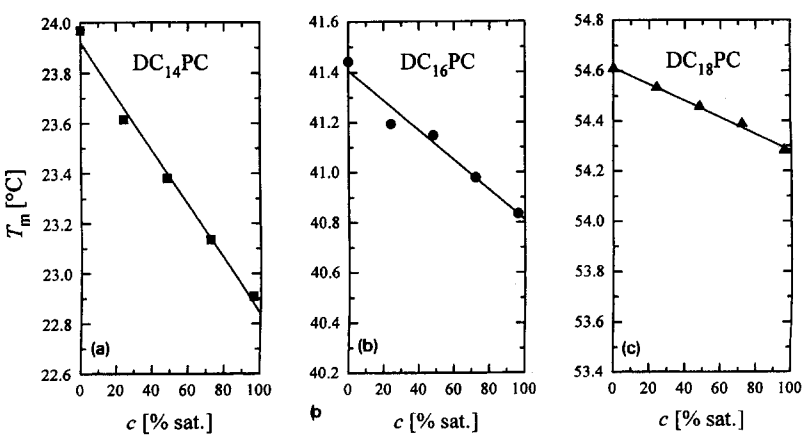

Fig. 6. Variation of the transition temperature, T_m, with the lindane concentration in multilamellar $DC_{14}PC$, $DC_{16}PC$, and $DC_{18}PC$ bilayers as determined from the position of the corresponding DSC high-temperature specific-heat peaks in Fig. 2.

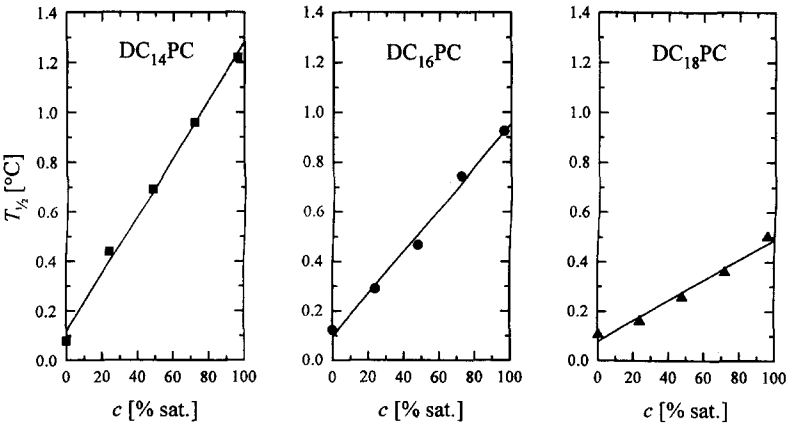

Fig. 7. Variation of the width, $T_{1/2}$, of the transition with the lindane concentration in multilamellar $DC_{14}PC$, $DC_{16}PC$, and $DC_{18}PC$ bilayers as determined from the width at half maximum of the corresponding DSC high-temperature specific-heat peaks in Fig. 2.

taining lindane as the position, T_m, of the main peak and denote by $T_{1/2}$ the width of the peak at half maximum. The results for T_m and $T_{1/2}$ for the three different lipid systems as a function of lindane concentration are given in Figs. 6 and 7. Both T_m and $T_{1/2}$ appear to depend linearly on the concentration of lindane in the full concentration range investigated for all three lipid species. In the case of T_m this observation is in accordance with classical thermodynamics for dilute solutions (freezing-point depression). The freezing-point depression is stronger the shorter the lipid acyl chains are. Similarly, there is a systematic increase in the degree of broadening as the acyl chain length is decreased. A linear dependence of $T_{1/2}$ on the concentration of foreign molecular compounds incorporated in lipid bilayers has been observed previously for the general anesthetics halothane and enflurane in $DC_{16}PC$ vesicles [27].

The total heat content, i.e., the transition enthalpy ΔH, of the equilibrium specific heat functions in Fig. 2 is plotted in Fig. 8 as a function of lindane concentration for the three different lipid species. In the case of $DC_{18}PC$ it was not possible to separate the main transition from the pre-transition and the ΔH given in Fig. 8 contain contributions to the transition enthalpy from both transitions. For all three phospholipids it is found that ΔH is independent of the lindane concentration within the accuracy of the measurements. The average values obtained for ΔH from Fig. 8 are 6.0 kcal/mol for $DC_{14}PC$, 8.3 kcal/mol for $DC_{16}PC$, and 11.1 kcal/mol for $DC_{18}PC$. These values compare reasonably well with values quoted in the literature [28]: 6.5 kcal/mol, 8.7 kcal/mol, and (1.8 + 10.4 kcal/mol).

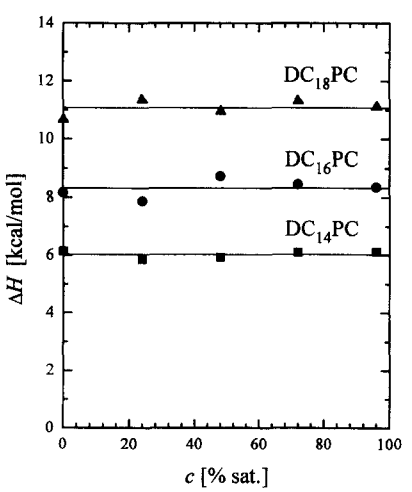

Fig. 8. Variation of the transition enthalpy, ΔH, with the lindane concentration in multilamellar $DC_{14}PC$, $DC_{16}PC$, and $DC_{18}PC$ bilayers as determined from the corresponding DSC high-temperature specific-heat peaks in Fig. 2.

5. Computer-simulation results

The purpose of the present computer simulation study is to examine the capability of the model in Eq. (1) to describe the systematics in the effects of partitioning of lindane into saturated diacylphosphatidylcholine lipid bilayers as a function of the acyl chain length. The attempt to use this model in describing the experimental data should also be seen as part of a strategy for developing a model for lipid–insecticide interactions. Since the values of the parameters involving lindane in the microscopic model in Eq. (1) is not known a priori, part of the simulation section will be concerned with effects due to variations of these parameters in order to find an optimal set of parameters for lindane. The properties of the model in the case of $DC_{16}PC$ bilayers has been studied in detail previously [16,18]. Specifically we want to investigate whether thermodynamic properties, that vary systematically with the acyl chain length, can be accounted for by the model. Of particular interest is to calculate the temperature dependence of the uptake of lindane, which is equivalent to the membrane/water partition coefficient, as well as the specific heat, both of which can be compared with experiments.

The computer-simulation results are presented in four subsections. At first, we discuss the case where the chemical potential is the same for all three lipid systems. Secondly, we allow the chemical potential to depend on the lipid in question. Thirdly, we investigate the effect of varying the parameters describing the interaction between lindane and the lipid bilayer. Finally, we show how the model simulations lead to insight into how lindane affects the acyl chain order, in particular the formation of kink states.

5.1. Keeping μ and lipid–lindane interaction parameters independent on chain length

The first set of simulations is carried out by using the same chemical potential, μ, the same lindane–lindane interaction parameter, J_{AA}, and the same set of lipid–lindane interactions, J^m_{LA}, for all three lipid species. The values used for J^m_{LA} are given in Table 2. The simulations for the different lipids only differs by the parameters describing the pure lipid bilayer, cf. Table 1. The simulation performed on $DC_{16}PC$ is the same as that of the previous study [18]. The chemical potential is taken to be $\mu = -0.94 \cdot 10^{-13}$ erg.

The results for the partition coefficient, x, and the specific heat, C_p, are shown in Fig. 9a and 9b. Fig. 9b also include specific-heat data for the pure phospholipid bilayers. The data in Fig. 9a suggest that the uptake of lindane from the water phase increases with increasing chain length. For all three chain lengths, x increases as the temperature is increased in the gel phase. In the cases of $DC_{16}PC$ and $DC_{18}PC$, x decreases at the main transition leading to a maximum of x just below T_m. Well into the fluid phase, x starts to increase again, but with a much smaller slope than in the gel phase. For $DC_{14}PC$ a maximum in x is not observed but there is a dramatic change in the rate of increase in x when the temperature is varied through the transition.

The specific-heat data in Fig. 9b show for all three lipid species that there is a broadening of the specific-heat peak and a concomitant shift in T_m as compared to the pure systems. The broadening is most pronounced in the case of $DC_{16}PC$ and least pronounced for $DC_{18}PC$, i.e., the broadening does not depend systematically on the length of the acyl chains. The shift in T_m is largest for $DC_{14}PC$ and smallest for $DC_{18}PC$, where the shift is actually upwards relative to the pure system.

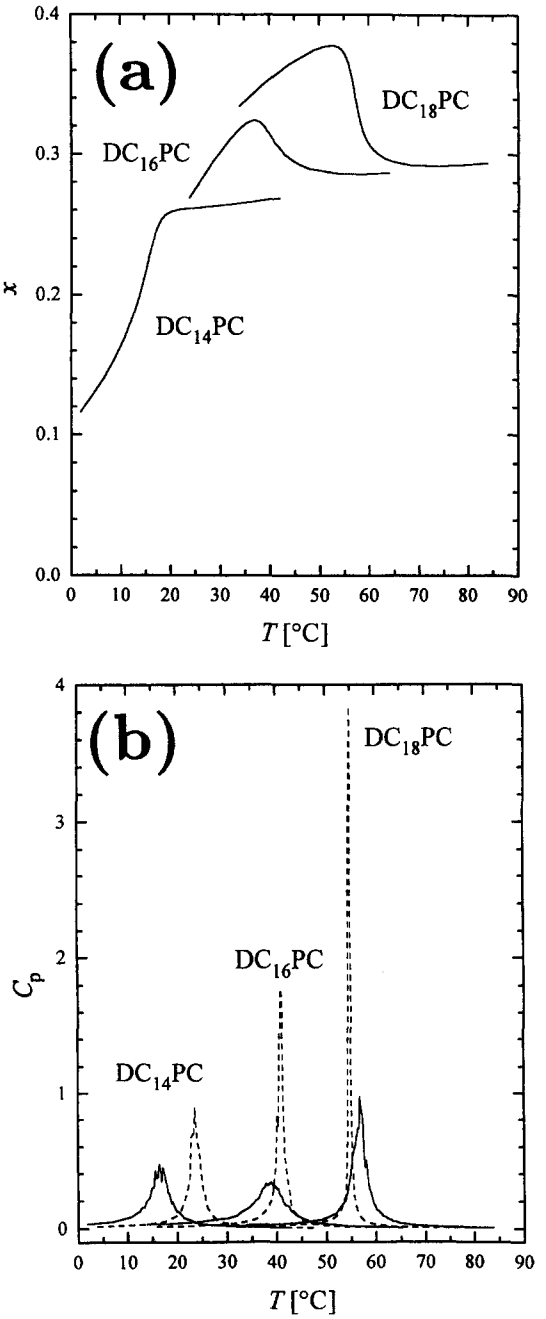

Fig. 9. Computer-simulation data for a model of $DC_{14}PC$, $DC_{16}PC$, and $DC_{18}PC$ lipid bilayers interacting with lindane. The model parameters characterizing lindane–lipid and lindane–lindane interactions are the same for all samples and the chemical potential is in all cases $\mu = -0.94 \cdot 10^{-13}$ erg. (a) Lindane partition coefficient, x, as a function of temperature. (b) Specific heat, C_p, as a function of temperature for lindane-containing bilayers (solid lines). For comparison, the specific-heat functions for the pure lipid bilayers are included (dashed lines).

5.2. Effects of varying μ

In the second set of simulations the lindane–lindane and the lipid–lindane interactions are taken to be the same for all three different lipid species, but the chemical potential is no longer equal for the three chain lengths. In the case of $DC_{14}PC$, μ has been increased from $-0.94 \cdot 10^{-13}$ erg to $-0.65 \cdot 10^{-13}$ erg and in the case of $DC_{18}PC$, μ has been reduced from $-0.94 \cdot 10^{-13}$ erg to $-1.35 \cdot 10^{-13}$ erg. μ remains unchanged in the case of $DC_{16}PC$. The strategy for choosing these values of μ for different chain lengths is justified a posteriori by the results found for the specific-heat curves (see below). The strategy assures that the derived partition coefficients reflect the experimental

fact that lindane has higher solubility in the lipids with the shorter acyl chains [4].

The partition coefficient and the specific heat for this set of parameters are presented in Fig. 10a and 10b, respectively. As a reference the specific heat for the pure systems are also included in Fig. 10b. The chain-length dependence of x is now opposite that in Fig. 9a: the uptake of lindane increases as the chain lenght is decreased. Furthermore, all three x-curves have a peak just below T_m. The peak is sharpest for the longest chain and

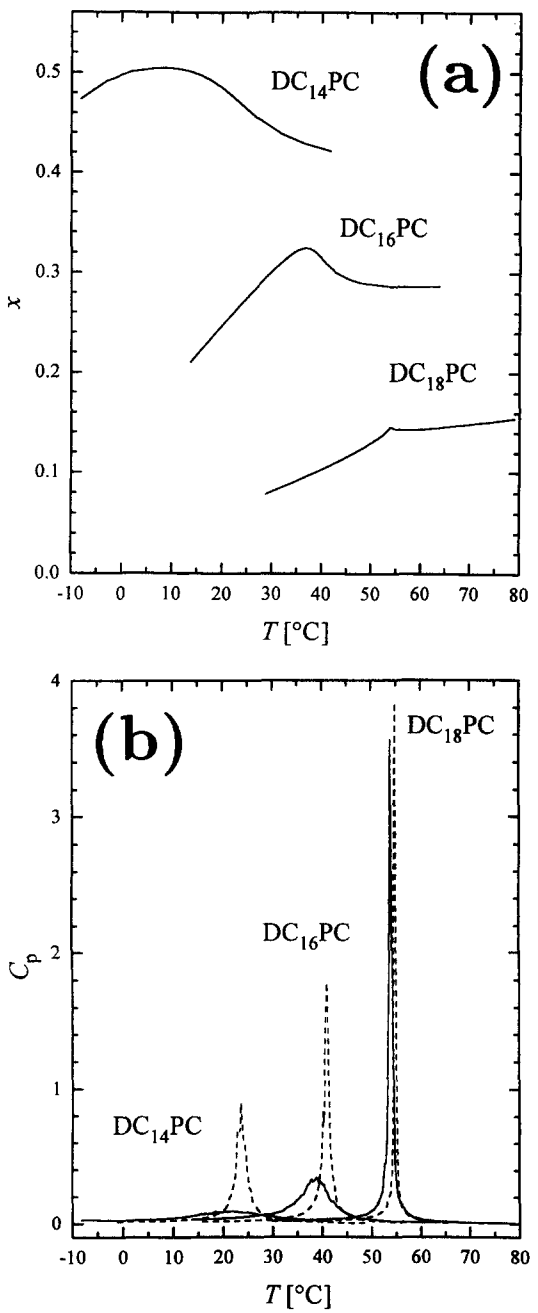

Fig. 10. Computer-simulation data for a model of $DC_{14}PC$, $DC_{16}PC$, and $DC_{18}PC$ lipid bilayers interacting with lindane. The model parameters characterizing lindane–lipid and lindane–lindane interactions are the same for all samples. The chemical potentials are $\mu = -0.65 \cdot 10^{-13}$, $-0.94 \cdot 10^{-13}$, and $-1.35 \cdot 10^{-13}$ erg for $DC_{14}PC$, $DC_{16}PC$, and $DC_{18}PC$, respectively. (a) Lindane partition coefficient, x, as a function of temperature. (b) Specific heat, C_p, as a function of temperature for lindane-containing bilayers (solid lines). For comparison, the specific-heat functions for the pure lipid bilayers are included (dashed lines).

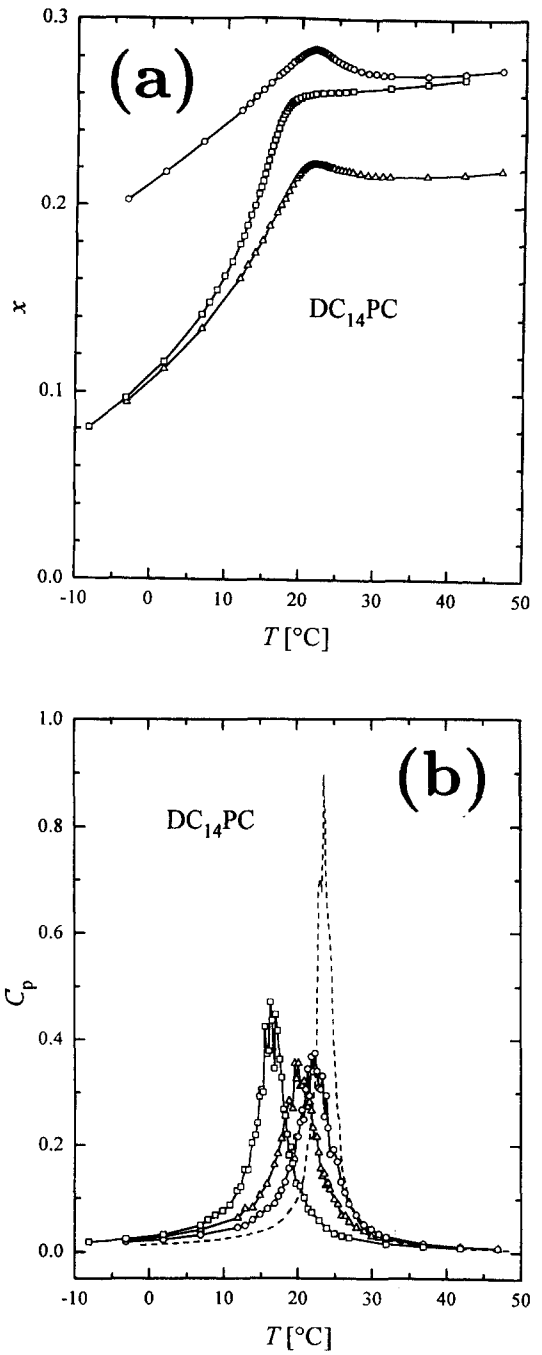

Fig. 11. Computer-simulation data for a model of $DC_{14}PC$ lipid bilayers interacting with lindane. The chemical potential is $\mu = -0.94 \cdot 10^{-13}$ erg. Effects are shown due to variations of the lipid–lindane interaction parameters, J^m_{LA}, in Table 2. The data set denoted by □ is our reference set that corresponds to the parameter values given in Table 2 (cf. Figs. 9a and 9b). The data set denoted by ○ is obtained by changing J^1_{LA} to $-0.20 \cdot 10^{-15}$ erg relative to the reference set. The data set denoted by △ is obtained by changing J^{10}_{LA} to $0.06 \cdot 10^{-14}$ erg relative to the reference set. (a) Lindane partition coefficient, x, as a function of temperature. (b) Specific heat, C_p, as a function of temperature for lindane-containing bilayers (solid lines). For comparison the specific heat function for the pure $DC_{14}PC$ bilayer is included (dashed line).

broadest for the shortest chain. The levels as well as the shapes of the x-curves for the $DC_{14}PC$ and $DC_{18}PC$ systems have been changed significantly upon changing the value of μ. This type of effect was also observed previously for the $DC_{16}PC$ system [18]. Turning to the specific-heat curves in Fig. 10b we now see that the broadening effect increases with decreasing chain length and the downwards shift in transition temperature, T_m, is increased with decreasing chain length of the lipid. The effect of lindane on the specific heat is now clearly largest for the $DC_{14}PC$ system and smallest for the $DC_{18}PC$ system.

5.3. Effects of varying the specific lipid–lindane interactions

In the third set of simulations we only consider $DC_{14}PC$ at a chemical potential $\mu = -0.94 \cdot 10^{-13}$ erg for lindane and allow the lipid–lindane interactions to vary. The results are presented in Fig. 11a and 11b for the partition coefficient and the specific heat, respectively. As a reference we use the results for the case in Fig. 9a and 9b (□). The curves marked by ○ are from an almost identical simulation, the only difference being that the value of J^1_{LA} has been changed from $-0.20 \cdot 10^{-13}$ erg to $-0.20 \cdot 10^{-15}$ erg, i.e., the interaction of lindane with the all-trans acyl chain state has been made less repulsive. Similarly, the only difference between the reference data set and the curves marked by △ is that the value of J^{10}_{LA} has been changed from $0.06 \cdot 10^{-13}$ erg to $0.06 \cdot 10^{-14}$ erg, i.e., the interaction of lindane with the fluid acyl chain state has been made less attractive.

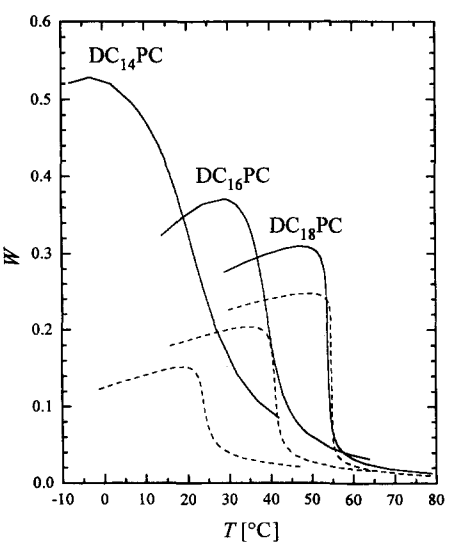

Fig. 12. Computer-simulation data for the acyl-chain kink probability, W, for lipid bilayers with (—) and without (– – –) lindane shown as a function of temperature. Results are shown for $DC_{14}PC$, $DC_{16}PC$, and $DC_{18}PC$ bilayers under the same conditions as in Fig. 10. The model parameters characterizing lindane–lipid and lindane–lindane interactions are the same for all samples. The chemical potentials are $\mu = -0.65 \cdot 10^{-13}$, $-0.94 \cdot 10^{-13}$, $-1.35 \cdot 10^{-13}$ erg for $DC_{14}PC$, $DC_{16}PC$, and $DC_{18}PC$, respectively.

It is observed, that either of the changes made in the interaction parameters can induce the presence of a peak in the partition coefficient. The level of the lindane concentration in the gel and fluid phases changes as expected. Decreasing the repulsion between lindane and the all-*trans* acyl chain state increases the level of lindane in the gel phase, but does not affect the level in the fluid phase. Similarly, decreasing the attraction of the fluid acyl chain state decreases the level of lindane in the fluid phase, without changing the level in the gel phase.

The specific-heat curves in Fig. 11b show that both of the changes cause the shift in T_m to be smaller than for the reference set of parameter values. Conversely, the broadening seems to be slightly larger for both cases of changed parameters. No obvious correlation is observed of either the broadening or the shift in T_m with the level of lindane. Instead the relative levels of lindane in the two phases appear to be of importance; the smaller the difference in the level of lindane in the two phases, the broader the peak and the smaller the shift in T_m.

5.4. Effect of lindane on acyl chain order and kink-state formation

The model in Eq. (1) proposed here to describe the interaction between lindane and lipid bilayers assumes that there is a specific attractive interaction between lindane and certain excited acyl chain states (states $m = 5$–9 in Table 2) [17,18]. These states have elements of kink excitations, i.e., subsequent formation of *gauche*$^-$ and *gauche*$^+$ rotations in the acyl chain [24]. State $m = 5$ is the pure kink state which turns out to be a dominant chain excitation in the pure bilayer transition [24,25]. The kink probability displays a maximum in the transition region [30]. The kink-state probability can be probed by Fourier transform infrared Raman spectroscopy [29].

In Fig. 12 are shown the computer-simulation data for the kink-state probability, W, for $DC_{14}PC$, $DC_{16}PC$, and $DC_{18}PC$ bilayer systems with and without lindane. The data are obtained for the same set of model parameters as used to generate the data in Fig. 10. It is observed that for all three systems there is a significant enhancement of the kink probability when lindane is incorporated into the bilayer. The enhancement is very strong for $DC_{14}PC$ bilayers and decreases for increasing chain length.

6. Discussion and conclusions

We have in this paper presented results from a combined experimental and model theoretical study of the effects of the insecticide lindane on saturated diacylphospholipid bilayers of different acyl chain length, $DC_{14}PC$, $DC_{16}PC$, and $DC_{18}PC$. The experiments involve DSC

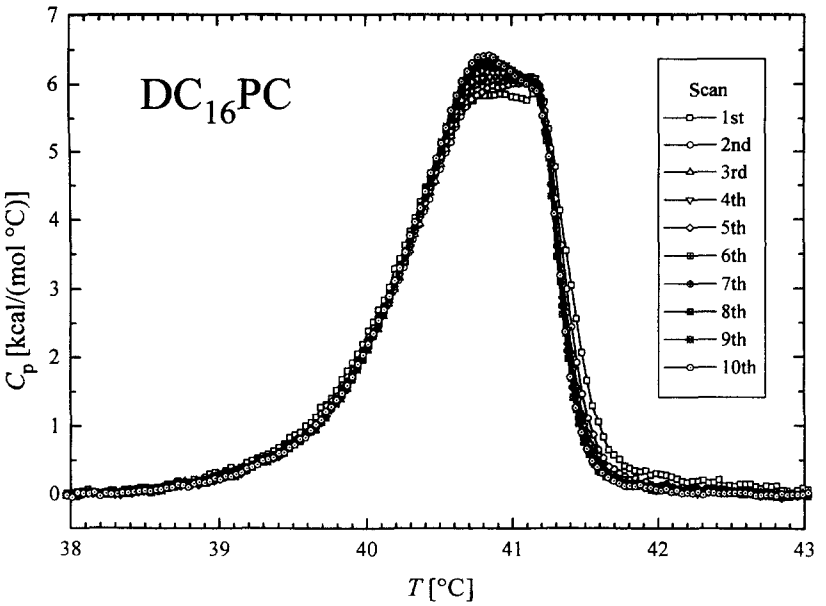

Fig. 13. Specific-heat data obtained for unilamellar bilayers of 240 μM $DC_{16}PC$ with a lindane concentration corresponding to 48% sat. Results from ten successive upscans are shown.

analysis of multilamellar vesicles. The theoretical calculations involve computer simulations on a simple and well-defined microscopic molecular interaction model. The combined set of results put us in a position to describe certain aspects of the effects of lindane on the physicochemical properties of lipid bilayers and to relate the macroscopic observed properties to microscopic phenomena, in particular dynamic membrane heterogeneity and selective interactions between lindane and the lipid acyl chain. Moreover, we propose that the kinetic effects observed in the DSC experiments could serve to guide our understanding of how insecticides are incorporated into lipid membranes. Although results are presented only for lindane, it is conceivable that the effects described are general for a large class of insecticides, including DDT, malathion, parathion together with lindane, and that the generic aspects of insecticide–lipid interactions is closely related to that of certain drugs such as halothane [27] and dibucaine [31].

6.1. Kinetics of lindane incorporation into multilamellar lipid bilayers

In order to discuss the observed kinetic effects in lindane interaction with lipid bilayers it is useful first to make the following general considerations. The lindane molecules are initially present in the aqueous phase in which the multilamellar vesicles are dispersed. In order to attain equilibrium, two processes have to take place. Lindane has to partition into the outermost lipid bilayer and it has to permeate through the whole multilamellar stack of bilayers in order to equilibrate with both the inner bilayers and the aqueous layers between the bilayers; the aqueous regions are simply not connected and the different water layers and the external aqueous reservoir can only equilibrate via passage of lindane across multiple lipid bilayers. The permeation of lindane through the bilayers will be faster in the transition region since it is expected that the transbilayer passive permeability of compounds like lindane displays a strong anomalous maximum at the phase transition [16,32]. This anomaly is related to the strong density fluctuations and the dynamic bilayer heterogeneity accompanying the transition [19,33], cf. Section 6.2 below. If the incorporation of lindane in lipid bilayers happens generally to be slow it is therefore expected that successive passes through the phase transition will help to make the outer chemical potential establish itself throughout the lamellar stack. However, as the transition is passed the partition coefficient of lindane changes substantially and lindane exchange between the lipid bilayer and the aqueous region has to take place. This leads to a considerable change in the concentration of lindane in the aqueous regions both as a function of temperature and the number of scans. Moreover, due to differences in bilayer curvature the partition coefficient is likely not to be the same for the inner and the outer bilayers in the multilamellar arrangement. These considerations exposes the key difficulties in dealing with partitioning of a molecular compound into multilamellar lipid systems and defining an equilibrium situation in relation to a DSC experiment: the lindane molecules are constantly on the move.

The experimental results presented in Figs. 1 and 3 show that some changes of multilamellar bilayer suspensions containing lindane take place when multiple successive scans are performed on the sample. What sort of changes we are dealing with is not a simple question to

answer, and we are unable to furnish an unambiguous explanation of the kinetic effects. Important problems to be resolved before such an explanation can be attempted involve determination of the actual chemical potential in the aqueous phase and how it may vary as the lindane solubility in the lipid phases changes with temperature as well as a clarification of the positioning of lindane in the bilayer and whether several lindane pools may exist. Even though we at present do not possess the information necessary to resolve these questions we shall in the remaining part of this section discuss various aspects of the problem.

It is likely that the observed kinetic effects are caused by the multilamellar structure of the vesicles. This is supported by DSC scans performed on samples consisting of only unilamellar lipid vesicles, an example of which is displayed for $DC_{16}PC$ in Fig. 13, showed very little dependence on the number of scans. A small deviation between the result of the very first scan and all the subsequent scans may be discerned. The reason for this could be (see also below) that the transbilayer passive permeability of lindane displays a maximum at the phase transition. Therefore, only after having been taken through the phase transition once has the aqueous lumen of the vesicle been receiving a substantial amount of lindane from the external aqueous lindane solution.

The intriguing observation made from the data for the lipid bilayer systems in Fig. 1 is that progression of the specific-heat function during successive scans is to diminish the shift relative to the transition temperature of the pure system. From the general considerations presented above one might have expected the opposite trend to occur, since more lindane will be incorporated into the inner bilayers as more scans are performed. It is entirely possible that the multilamellar sample never reaches true equilibrium. It is also possible that phase separation and cooperative effects due to the interlamellar interactions play a role. The occurrence of two peaks, which keep almost the same peak positions for a series of successive scans, supports this possibility. The special effect observed in Fig. 3 following a break in the series of upscans and subsequent resting at a low temperature may provide a clue to resolving these questions.

There might also be an influence from the breaking up of the individual layers due to the interlamellar strain that is created in the transition region when the bilayer area expands 10–15%. Furthermore, as remarked above, the chemical potential and partition coefficient is likely to depend on the bilayer curvature so that high curvatures prevent lindane uptake. This could be important, since we expect the inner layers to be of a much higher curvature than the outer layers. Finally, the possibility remains that lindane incorporates into bilayers in different populations, e.g. in different positions in the bilayer, and the relative amount of the populations depends on the thermal history and the equilibration time. It should be possible to investigate the positioning of lindane in the bilayer by fluorescence-quenching techniques as has been done for other hydrophobic species [34].

The last scans of each series of specific-heat data in Fig. 2 show some general properties of lipid–lindane interactions. First of all, $DC_{14}PC$ is much more influenced by lindane than $DC_{16}PC$ and $DC_{18}PC$, both concerning the broadening of the peak and the shift of T_m. According to Antunes-Madeira and Madeira [4] the lindane partitioning into the membrane is much larger for $DC_{14}PC$ than for $DC_{16}PC$ and $DC_{18}PC$. Taking this fact into account it is possible that the progressively stronger influence of lindane on the specific heat for decreasing chain length is a mere concentration effect. Experimental values for partition coefficients are, however, too uncertain to draw final conclusions. Secondly, we have found that the transition enthalpy, ΔH, does not depend upon the lindane concentration. This indicates very strongly that the specific volume of lindane in lipid bilayers is vanishingly small.

6.2. Modelling lipid–lindane interactions

The finding of significant kinetic effects in the experimental specific-heat data makes it difficult to perform a quantitative comparison with the computer-simulation data obtained for the model in Eq. (2). Hence, we are not at present in a position to fully evaluate the quantitative capability of the model to describe the experimental system. However, we can make a qualitative comparison between the predictions of the model and the experimental data of the present paper and the general trends in the partition coefficients measured by Antunes-Madeira and Madeira [4]. Such a comparison may help towards building a more complete theoretical model.

The first set of simulation results shown in Fig. 9 is not in qualitative accordance with the experimental observations. The systematic variation of the specific-heat curves with chain length is absent. Furthermore, the systematics in the partition coefficient is opposite to that measured [4]. The larger uptake for the longer chains found in the model simulations is probably due to the higher degeneracy, D_m, of the intermediate and fluid states for the longer chains.

The second set of simulation results displayed in Fig. 10 resembles the experimental results more closely. The systematic variation of both the specific heat and the partition coefficient, x, with the length of the chain is the same in simulation and experiment. The relative width of the peaks in the specific-heat curves are found to be larger for the shorter chain, as are the shifts in T_m. In both experiment and simulation, the width of the peak in the x- and C_p-curves are comparable. This implies that the uptake of lindane is related to the increased fluctuations in the phase transition region, i.e., the larger wings in the specific-heat function.

In the model we use, the chemical potential, μ, is associated with the water phase, i.e., it is a measure of the

concentration of lindane in the water phase. To compare the results of how lindane interacts with different kinds of lipid bilayers, the value of μ must be the same. In the second set of simulations discussed above, μ was allowed to vary for the different lipid species. The third set of simulation data displayed in Fig. 11 was obtained for fixed value of μ. The data set shows that a peak in the partition coefficient can be obtained from the model, provided that the parameters describing the interaction between lindane and the bulk lipid phases are appropriately adjusted. This suggests that we might be able to choose the interaction parameters, such that the systematics observed in the second set of simulations would be obtained using the same chemical potential for all three lipid systems. A necessary input for making this adjustment would be reliable experimental values for the equilibrium partition coefficient and its temperature dependence. Unfortunately, the available experimental partition coefficients for lindane in the bulk gel and fluid lipid phases [4] are, as indicated in Section 6.1, possibly invalidated by kinetic effects.

6.3. Enhanced lindane absorption and dynamic membrane heterogeneity

Experimental measurements of the partition coefficients of lindane in $DC_{14}PC$, $DC_{16}PC$, and $DC_{18}PC$ indicates that there is an enhanced absorption in the transition region and that the absorption is stronger for the lipid bilayer with the shortest lipid chains. As we have discussed above, the model proposed in Eq. (1) for lipid–lindane interactions is capable of reproducing this behavior, at least qualitatively. The incorporation of foreign molecular compounds into lipid bilayers and the trans-bilayer permeation of these compounds correlates with the degree of fluctuations in the bilayer membrane [15,16,19,32,35]. Shorter acyl chains are known to sustain stronger fluctuations [26]. Computer-simulation calculations of the type employed in the present work have shown for drugs [16] as well as for compounds like insecticides [36] that the fluctuations are accompanied by dynamic lipid-domain formation on a nanoscopic scale of 10–1000 Å [33]. The dynamic heterogeneity, which is most dramatic in the transition region, facilitates incorporation of insecticides like lindane and is responsible for the enhanced absorption in the transition region. The heterogeneous states may pictorially be described in terms of a bulk equilibrium phase embedded with lipid domains of a structure resembling the opposite phase. The resulting heterogeneous pattern is dynamic and characterized by fluctuating interfaces separating the domains and the bulk. These interfaces are known from simulations to be rich in defects, such as kink excitations [37]. Consequently, the insecticide molecules are adsorbed predominantly at these interfaces leading to increased heterogeneity. The insecticide acts in this way quite similar to an emulsifier. A similar effect has been discussed to arise for certain drugs [16] which have been found to accumulate in the interfaces. Since in the present case, the lindane molecules are selectively attracted to the excited acyl chain states, cf. Table 2, the presence of lindane in the bilayer leads to an enhancement in e.g. the kink probability as was shown in Fig. 12. It would be interesting to test this specific prediction, e.g., by Fourier infrared Raman spectroscopy.

6.4. Concluding statements

Obviously, the theoretical model proposed in this paper for the lipid–lindane system is not a complete model of the system, but it is likely that the essential features of lindane–lipid interactions are captured by this model, in particular with respect to describing the effects as a function of lipid acyl chain length. It should be possible, however, to refine the model when more reliable experimental data becomes available for properties, such as the equilibrium temperature dependence of the partition coefficients, that could be used to fix the values of some of the model parameters.

The experimental results presented in this paper show that the incorporation of lindane into multilamellar lipid bilayer membranes is subject to some very severe kinetic effects. It is likely that similar effects will be present for other insecticides previously studied, such as DDT, parathion, and malathion [10,12,14]. The kinetic effects discovered suggest that published data for partition coefficients of lindane in multilamellar phospholipid bilayers in the gel phase [4] may not represent true equilibrium. Our results show that kinetic effects of lindane incorporation is present in the case of multilamellar vesicles hence suggesting that unilamellar lipid assays may be more useful for the study of effects of insecticides on the lipid-bilayer component of cell membranes.

Acknowledgements

This work was supported by the Danish Natural Science Research Council under an operating (SNF-11-0065) and an equipment grant (SNF-11-9560-1). Enlightening discussions with Rodney L. Biltonen are gratefully acknowledged.

References

[1] Lakowicz, J.R. and Hogen, D. (1980) Chem. Phys. Lipids 26, 1–40.
[2] Brooks, G.T. (1974) Chlorinated Insecticides, Vol. I, pp. 12–15, CRC Press, Cleveland, OH.
[3] Rubin, E., Miller, K.W. and Roth, S.H. (eds.) (1991) Molecular and Cellular Mechanisms of Alcohols and Anaesthetics, Ann. New York Acad. Sci. Vol. 625.
[4] Antunes-Madeira, M.C. and Madeira, V.M.C. (1985) Biochim. Biophys. Acta 820, 165–172.
[5] Antunes-Madeira, M.C., Almeida, L.M. and Madeira, V.M.C. (1989) Biochim. Biophys. Acta 982, 161–166.

[6] Antunes-Madeira, M.C. and Madeira, V.M.C. (1990) Biochim. Biophys. Acta 1022, 110–114.
[7] Buff, K. and Berndt, J. (1981) Biochim. Biophys. Acta 643, 205–212.
[8] Packham, E.D., Thompson, J.E., Mayfield, C.I., Inniss, W.E. and Kruuv, J. (1981) Arch. Environ. Contam. Toxicol. 10, 347–356.
[9] Buff, K., Bründl, A. and Berndt, J. (1982) Biochim. Biophys. Acta 688, 93–100.
[10] Antunes-Madeira, M.C. and Madeira, V.M.C. (1990) Biochim. Biophys. Acta 861, 159–164.
[11] Antunes-Madeira, M.C. and Madeira, V.M.C. (1990) Biochim. Biophys. Acta 1023, 469–474.
[12] Antunes-Madeira, M.C. and Madeira, V.M.C. (1990) Biochim. Biophys. Acta 778, 49–56.
[13] Antunes-Madeira, M.C., Videira, R.A. and Madeira, V.M.C. (1994) Biochim. Biophys. Acta 1190, 149–154.
[14] Antunes-Madeira, M.C. and Madeira, V.M.C. (1994) Biochim. Biophys. Acta 901, 61–66.
[15] Mouritsen, O.G. (1991) Chem. Phys. Lipids 57, 179–194.
[16] Jørgensen, K., Ipsen, J.H., Mouritsen, O.G. and Zuckermann, M.J. (1993) Chem. Phys. Lipids 65, 205–216.
[17] Jørgensen, K., Ipsen, J.H., Mouritsen, O.G., Bennett, D. and Zuckermann, M.J. (1991) Biochim. Biophys. Acta 1062, 227–238.
[18] Jørgensen, K., Ipsen, J.H., Mouritsen, O.G., Bennett, D. and Zuckermann, M.J. (1991) Biochim. Biophys. Acta 1067, 241–253.
[19] Mouritsen, O.G. and Jørgensen, K. (1992) BioEssays 14, 129–136.
[20] Mouritsen, O.G. and Jørgensen, K. (1994) Chem. Phys. Lipids 73, 3–25.
[21] Mayer. L.D., Hope, M.J. and Cullis, P.R. (1986) Biochim. Biophys. Acta 858, 161–168.
[22] McKay, D. and Leinonen, P.J. (1975) Environ. Sci. Technol. 9 (13), 1178–1180.
[23] Hollifield, H.C. (1979) Bull. Environ. Contam. Toxicol. 23, 579–586.
[24] Pink, D.A., Green, T.J. and Chapman, D. (1980) Biochemistry 19, 349–356.
[25] Mouritsen, O.G. (1990) in Molecular Description of Biological Membrane Components by Computer Aided Conformational Analysis (R. Brasseur, ed.), Vol. 1, pp.3–83, CRC Press, Boca Raton, FL.
[26] Ipsen, J.H., Jørgensen, K. and Mouritsen, O.G. (1990) Biophys. J. 58, 1099–1107.
[27] Mountcastle, D.B., Biltonen, R.L. Halsey, M.J. (1978) Proc. Natl. Acad. Sci. USA 75, 4906–4910.
[28] Lasic, D. (1993) Liposomes: From Physics to Applications, Elsevier, Amsterdam.
[29] Mendelsohn, R., Davies, M.A., Brauner, J.W., Schuster, H.F. and Dluhy, R.A. (1989) Biochemistry 28, 8934–8939.
[30] Mouritsen, O.G., Boothroyd, A., Harris, R., Jan, N., Lookman, T., MacDonald, L., Pink, D.A. and Zuckermann, M.J. (1983). J. Chem. Phys. 79, 2027–2041.
[31] Van Osdol, W.W., Ye, Q., Johnson, M.L. and Biltonen, R.L. (1992) Biophys. J. 63, 1011–1017.
[32] Mouritsen, O.G., Jørgensen, K. and Hønger, T. (1994) in Permeability and Stability of Lipid Bilayers (Disalvo, E.A. and Simon, S.A., eds.), pp. 84–112, CRC Press, Boca Raton, FL.
[33] Mouritsen, O.G. and Jørgensen, K. (1994) Mol. Membr. Biol. (in press).
[34] Michelangeli, F., Robson, M.J., East, J.M. and Lee, A.G. (1990) Biochim. Biophys. Acta 1028, 49–57.
[35] Mouritsen, O.G. and Biltonen, R.L. (1993) in Protein–Lipid Interactions. New Comprehensive Biochemistry (Watts, A., ed.), Vol. 25, pp. 1–39.
[36] Sabra, M.C., Jørgensen, K. and Mouritsen, O.G. (1994) (in preparation).
[37] Cruzeiro-Hansson, L. and Mouritsen, O.G. (1988) Biochim. Biophys. Acta. 944, 63–72.